Materials Today Bio 33 (2025) 101957

Contents lists available at ScienceDirect

Materials Today Bio

journal homepage: www.journals.elsevier.com/materials-today-bio

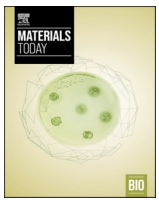

Silk fibroin hydrogel with recombinant silk fibroin/NT3 protein enhances wound healing by promoting type III collagen synthesis and hair follicle regeneration in skin injury

Yingying Yan [a], Mingxuan Li [b], Longyu Guo [b], Wenxue Zhang [b], Ronghua Wu [b], Tuchen Guan [b], Jue Ling [b], Yumin Yang [b], Mei Liu [b,*], Xiaosong Gu [b,**], Yan Liu [b,***]

[a] Key Laboratory of Neuroregeneration of Jiangsu and Ministry of Education, Co-innovation Center of Neuroregeneration, NMPA Key Laboratory for Research and Evaluation of Tissue Engineering Technology Products, Nantong University, and Research Center of Clinical Medicine, Affiliated Hospital of Nantong University, China
[b] Key Laboratory of Neuroregeneration of Jiangsu and Ministry of Education, Co-innovation Center of Neuroregeneration, NMPA Key Laboratory for Research and Evaluation of Tissue Engineering Technology Products, Nantong University, China

ARTICLE INFO

Keywords:
Silk fibroin hydrogel
Neurotrophin-3
Skin injury
Type III collagen
Scar

ABSTRACT

Scar formation on skin wounds remains a considerable challenge in regenerative medicine. Various wound dressings, composed of biomaterials alone or in combination with bioactive factors, have been developed to improve healing outcomes. In this study, we designed a recombinant neurotrophin-3 (NT3) containing a silk fibroin light chain (SFL) and developed a silk fibroin (SF) hydrogel with NT3 activity. The SFL-NT3 protein bound to the heavy-light chains of SF and was efficiently integrated into the SF hydrogel. We evaluated the effect of the recombinant NT3-SFL hydrogel on wound healing in a mouse skin injury model. This hydrogel enhanced wound healing. Remarkably, SFL-NT3 increased the levels of type III collagen (Col3) during the healing process and induced hair follicle formation, which is a characteristic of scar-less healing. Further investigation revealed that SFL-NT3 upregulated Col3 expression in skin fibroblasts expressing the NT3 receptor, TrkC. NT3 activation of TrkC leads to Akt phosphorylation, resulting in elevated Sox2 levels, which in turn enhances Col3 transcription. Notably, TrkC inhibition abrogated the beneficial effects of SF + SFL-NT3 on wound healing, confirming its involvement in this signaling pathway. In conclusion, the SF hydrogel loaded with SFL-NT3 facilitated rapid and reduced scarring during wound healing, providing a promising approach for the clinical treatment of SF-based biomaterials that incorporate bioactive factors.

1. Introduction

The skin, the largest multi-layered organ in the human body, serves as a key barrier against excessive water loss and pathogen invasion [1–3]. Skin wound repair is a complex regenerative process comprising three overlapping phases: homeostasis and inflammation; cell proliferation and tissue replacement; and remodeling, maturation, and decomposition [4,5]. Severe injuries lead to fibrous scar formation, and complete skin wound healing requires both dermal repair and regeneration of skin appendages, including hair follicles and sebaceous glands [6,7], which remains a challenge in cases of significant injury. Autologous or allogeneic skin transplantation is often performed to achieve scar-free healing. However, the limited availability of donor tissue hampers the widespread adoption of this technique [8].

Tissue-engineered materials offer promising alternatives for scar-free skin healing. Various natural and synthetic skin substitutes are used for cutaneous wound repair [9]. Silk fibroin (SF), a natural protein, has gained considerable attention in tissue engineering because of its outstanding biocompatibility [10,11], highlighting its potential for extensive applications in tissue-engineering products. Moreover, SF can be modified with peptides, proteins, and other bioactive molecules to enhance its tissue repair properties. Scar formation remains a substantial challenge in skin injury, as it severely impedes functional recovery. Various wound cell lineages including keratinocytes, fibroblasts,

* Corresponding author.
** Corresponding author.
*** Corresponding author.
E-mail addresses: liumei@ntu.edu.cn (M. Liu), nervegu@ntu.edu.cn (X. Gu), liuyan@ntu.edu.cn (Y. Liu).

https://doi.org/10.1016/j.mtbio.2025.101957
Received 19 February 2025; Received in revised form 8 May 2025; Accepted 6 June 2025
Available online 9 June 2025

adipocytes, and cutaneous nerves contribute to scar deposition. Bioactive molecules targeting these cell types hold promise for influencing the wound-healing process.

This study investigated the effects of a recombinant protein that combines neurotrophic factor NT3 and the light chain of SF on skin healing in a mouse model. The underlying rationale for this approach stems from the understanding that innervation is critical for wound re-epithelialization [12,13]. Additionally, successful innervation plays a pivotal role in the epimorphic regeneration of limbs in organisms such as axolotls, suggesting a potential therapeutic role for neurotrophic factors in wound healing. Neurotrophic factors, initially identified in the nervous system, are essential for the development, maintenance, and regeneration of nerve fibers [14,15]. These factors include nerve growth factor (NGF), brain-derived neurotrophic factor (BDNF), NT-3, and NT-4, with NT-3 being extensively studied for its role in neurotrophy and neurite outgrowth. Referring to our previous studies [16], we conjugated NT3 and SFL, named SFL-NT3 to prepare a hydrogel containing SF and SFL-NT3. As anticipated, this SF hydrogel substantially accelerated skin wound healing Surprisingly, NT3 not only facilitated the innervation of the wounded tissue but also influenced collagen deposition and hair follicle formation during the healing process. This study further examined how SFL-NT3 modulates the expression of embryonic type III collagen, ultimately leading to improved scarless healing outcomes.

2. Materials and methods

2.1. Preparation of silk fibroin (SF) hydrogel

SF methacryloyl (Engineering for Life, China) at concentrations of 0.01 g, 0.05 g, and 0.1 g were weighed and dissolved in 1 mL of photoinitiator (Engineering for Life, China) to prepare 1 %, 5 %, and 10 % SF solutions respectively at room temperature. After stirring, the solutions were filtered through a 0.22 μm sterile needle filter for sterilization. Then, 2 μL SFL-NT3(100 μg/mL) was drawn into 1 mL silk fibroin solution, and 30 μL mixture were dropped onto coverslips (10 mm in diameter) and irradiated with 405 nm light source for 5 min to make the SF + SFL-NT3 hydrogel.

2.2. Scanning electron microscope imaging

For crosslinking, 30 μL of each 1 %, 5 %, and 10 % SF plus SFL-NT3 solution was placed in 24-well plates and exposed to 405 nm light for 5 min. The samples were frozen at − 80 °C for 1 d and then lyophilized for 1 d. Following lyophilization, aluminum sample mounting pieces (1-inch in diameter) were attached to the samples using conductive carbon strips. The samples were loaded into a vacuum chamber of a Hitachi S-4800 scanning electron microscope (SEM) (Tokyo, Japan) and scanned at an accelerating voltage of 3–5 kV and 12 μA.

2.3. Evaluation of NT3 release

The release profile of SFL-NT3 or NT3 from the SF hydrogel was assessed using an NT3 ELISA kit according to the manufacturer's instructions. The 1 %, 5 %, and 10 % SF plus SFL-NT3 solutions were placed in 24-well culture plates, irradiated with a 405 nm light source to form the hydrogel, and then 2 mL of PBS was added. The samples were incubated at 37 °C for different time points (1, 3, 5 days). At each time point, the supernatant was collected and stored, and fresh PBS was replenished. The NT3 concentration in the collected supernatants was measured using an ELISA kit and the absorbance at 450 nm was recorded using a microplate reader.

2.4. Cell culture

Mouse fibroblasts (L929 cells) were obtained from the Shanghai Cell Bank and cultured in Dulbecco's modified Eagle's medium (DMEM) supplemented with 10 % fetal bovine serum and 1 % P/S (ScienCell, 0503) in a humidified incubator at 37 °C with 5 % CO2. All the experiments were conducted using L929 cells within the first five passages.

2.5. Animal model

ICR mice were obtained from the Experimental Animal Center of Nantong University. Mice were randomly divided into three groups. All animals were anesthetized with isoflurane in oxygenated air using a small animal anesthesia machine and placed in a prone position on a temperature-controlled platform. The fur around the surgical site was shaved using an electric animal shaver and using depilation cream. A circular skin wound (10 mm diameter) was created on the back of each mouse. Subsequently, 50 μL of PBS, 5 % SF, or 200 ng/mL SF + SFL-NT3 was applied to the wound site for each mouse. The SF and SF + SFL-NT3 groups were then irradiated with a 405 nm UV fluorescent agent flashlight for 5 min to form the hydrogel. In subsequent rescue experiments, an additional group receiving SF + SFL-NT3+LPM4870108 was introduced, with the LPM4870108 concentration set at 0.2 nM. Wound healing was monitored and photographed at specific time points, and the wound area was quantified using the ImageJ software. Mice were euthanized on days 5 and 28 post-treatment, and the wound tissue along with a 2-mm border of healthy surrounding skin was excised for further analysis.

2.6. Histopathological observation

Histological sections were prepared from the excised tissues on days 5 and 28 post-wounding. The specimens, including wound tissue and 2-mm unwounded skin borders, were fixed in 4 % paraformaldehyde for 16 h and subsequently dehydrated using a graded series of sucrose solutions. Tissue blocks were sectioned into 12 μm slices, mounted on glass slides, and stained with hematoxylin and eosin (H&E). Masson's trichrome staining was performed to assess total collagen accumulation following the manufacturer's instructions. Morphological changes in the skin tissue were examined using light microscopy, and images were captured. The percentage area of collagen deposition was quantified using the ImageJ software.

2.7. Immunocytochemistry

Immunofluorescence (IF) assays were conducted our previous protocol [17]. After 48 h of culture, the L929 cells were fixed with 4 % paraformaldehyde for 20 min at room temperature, followed by three washes with PBS. Tissue blocks were sectioned into 12 μm slices. Cells or slices were then incubated with 10 % normal goat serum for 120 min at 37 °C, followed by overnight incubation at 4 °C with primary antibodies: anti-Col1 (rabbit, 1:200, Abcam, Cat. ab270993) and anti-Col3 (rabbit, 1:2000; Abcam, Cat. ab7778) and anti-p-TrkC (1:200; Abcam, Cat. ab240651), anti-Sox2 (Rabbit, 1:400; Cell Signaling Technology, Cat. 23064). The samples were then incubated with the corresponding secondary antibodies (Cy3-conjugated goat anti-rabbit and Alexa Fluor 488-conjugated goat anti-mouse, 1:400; Jackson ImmunoResearch) for 2 h at room temperature. All cells or tissues were counterstained with Hoechst 33342 (1:2000). Imaging was performed under a fluorescence microscope (Leica Biosciences). Images were converted to a 16-bit TIFF format, and regions of interest were selected for mean fluorescence intensity analysis using ImageJ software.

2.8. Single-cell RNA sequencing (scRNA-seq) analysis of public data GEO: GSE142471

ScRNA-seq data from Haensel et al. (GEO: GSE142471) were downloaded from the GEO repository. Two uninjured and three injured skin samples were integrated and submitted to PersonalBio for

subsequent analyses.

2.9. Western blotting

For Western blot analysis, L929 cells were cultured with or without SFL-NT3 (100 ng/mL) for 48 h. After three PBS washes, cells were lysed for 30 min at 4 °C in RIPA buffer containing protease and phosphatase inhibitor cocktails (Roche, Basel, Switzerland). The supernatant was collected after centrifugation at 13,000 rpm for 15 min, and the protein concentration was quantified using a BCA assay. Proteins were separated by 10 % SDS-PAGE and transferred onto a PVDF membrane (Millipore). The membrane was blocked with 5 % skim milk powder in Tris-buffered saline (TBS) and incubated overnight with the following primary antibodies: anti-Col3 (rabbit, 1:1000, Abcam, Cat. ab7778), anti-Col1 (rabbit, 1:1000, Abcam, Cat. ab270993), anti-Sox2 (rabbit, 1:1000; Cell Signaling Technology, Cat. 23064), anti-p-Sox2 (rabbit, 1:1000; ECM Bioscience, Cat. SP5521), anti-β-actin (mouse, 1:1000, Abcam, Cat. ab8226). After washes, the membrane was incubated with HRP-conjugated secondary antibodies (1:2000, anti-mouse, Beyotime, Cat# A0216; anti-rabbit, Beyotime, Cat# A0208) at 37 °C for 100–120 min. Immunoreactive bands were visualized using a chemiluminescent solution (Tanon, #180–5001) and detected.

2.10. Luciferase reporter assay

The cDNA fragment encoding mouse Sox2 was cloned into the pcDNA3.1 vector (General Biologicals, Anhui, China) as described in our previous study [18]. The promoter regions of Col3 were analyzed using the Jaspar and Animal TFDB (v3.0) databases, and potential transcription factor binding sites were identified. The Col3 promoter plasmid was constructed by cloning the mouse Col3 promoter from −1000 to +1 bp into the pGL4.1-basic luciferase reporter vector (General Biologicals). Human embryonic kidney cell line 293T (HEK-293T) was inoculated into 24-well plates at 8×10^4 cells per each well. After 16 h of culture, the Col3 promoter plasmid + pcDNA3.1, or pcDNA3.1-Sox2, was transfected for 48 h using the lipo8000TM transfection reagent. The fluorokinase activity was measured using a dual-luciferase reporter system (Promega).

2.11. Chromosome immunoprecipitation (ChIP)

ChIP assays were performed using an enzymatic Chromatin IP Kit (CST) according to the manufacturer's instructions as described in our previous study [19]. Briefly, mouse fibroblast L929 cells were fixed in 37 % formaldehyde for 10 min at room temperature, and glycine-unreacted formaldehyde was added for quenching. The cells were washed with PBS and collected. The cells were sonicated three times for 20 s each. A small fraction of the sonicated material was retained as a sample, and the remainder was incubated with antibodies against Sox2 or IgG. Immunoprecipitation complexes were collected using agarose protein beads and washed with elution buffer. Associated proteins, DNA complexes of reverse 30 min under 65 °C, and then use 65 M NaCl and 2 μL proteinase K treatment under 65 °C for 2 h. DNA was extracted using a wash buffer. The pellets were suspended in a wash solution and subjected to PCR amplification. The primers used in this study are listed in Table 1.

2.12. Molecular weight and specifications of chemicals

The molecular weight of the Trk inhibitor LPM4870108 is 410.4 and the usage concentration is 0.2 nM. The molecular weight of Akt inhibitor MK2206 is 443.93 and the usage concentration is 1 μM.

2.13. Statistic analysis

GraphPad Prism 5.0 software (GraphPad Software Inc., La Jolla, CA) was used for statistical analysis. All data were expressed as the means ± standard errors (SEs). Statistical significance between two datasets was tested using an unpaired two-tailed Student's t-test. One-way ANOVA was used to compare data from multiple groups. $P < 0.05$ was considered statistically significant.

Table 1
The sequences of primers.

Name	Sense (5′-3′)	Antisense (5′-3′)
Chip-Col3	CCTATGTGTTTCTGTCATGCAAA	AGAAACAGCACATCTGGAGCAT
Col1	GCTCCTCTTAGGGGCCACT	CCACGTCTCACCATTGGGG
Col3	CTGTAACATGGAAACTGGGGAAA	CCATAGCTGAACTGAAAACCACC
NGF	CAGTGTCAGTGTGTGGGTTG	CTCTCTACAGGATTCGGGGC
FGF1	GCTCGCAGACACCAAATGAA	TTTCTGGCCGTAGTGAGTCC
FGF2	GAACCGGTACCTGGCTATGA	CAGTTCGTTTCAGTGCCACA
FGF7	TGAACTGTTCTAGCCCCGAG	CCACAATTCCAACTGCCACA
FGF8	ACCGGTCTGTACATCTGCAT	TTGCGGGTAAAGGCCATGTA
FGF9	AGGAGTGCGTGTTCAGAGAA	TTCTGGTGCCGTTTAGTCCT
FGF10	TGTTGCTGCTTCTTGTTGCT	GCTGGAAGGAGAGGAGAAGG
18s	CGCGGTTCTATTTTGTTGGT	CCTCCGACTTTCGTTCTTGA

3. Results

3.1. Fabrication and characterization of the SF + SFL-NT3 hydrogel

The hydrogel fabrication process is illustrated in Fig. 1A. The effects of SF and SFL-NT3 on wound healing were evaluated in a mouse model of full-thickness skin injury. Previous studies have demonstrated that recombinant SFL-NT3 forms a complex with SFH (SFH-SFL-NT3), similar to the natural SFH-SFL complex in SF. Based on this, an SF hydrogel incorporating SFL-NT3 was designed to enhance wound healing. Hydrogels with various SF concentrations (1 %, 5 %, and 10 %) were fabricated. All the SF hydrogels were white, flat, and uniform in appearance. Electron microscopy analysis revealed that the pore diameters of 5 % SF + SFL-NT3 (40.09 ± 2.4 μm) and 10 % SF + SFL-NT3 (39.7 ± 2.9 μm) hydrogels were significantly smaller than those of the 1 % SF + SFL-NT3 hydrogel (50.52 ± 3.4 μm) (Fig. 1B a, b). All hydrogel samples exhibited hydrophilic properties, with the 5 % and 10 % SF + SFL-NT3 hydrogels demonstrating higher contact angles than the 1 % SF + SFL-NT3 hydrogel (Fig. 1C a, b). Additionally, the release profiles of SFL-NT3 from the 1 %, 5 %, and 10 % SF + SFL-NT3 hydrogels were evaluated. Additionally, the release profiles of SFL-NT3 from the 1 %, 5 %, and 10 % SF + SFL-NT3 hydrogels were evaluated. However, the release from the 1 % SF group was rapid, while the 10 % SF group exhibited a relatively slower release compared to the other groups. The 5 % SF + SFL-NT3 hydrogel provided moderate and steady release (Fig. 1D a); thus, 5 % SF + SFL-NT3 was selected for subsequent experiments. Further investigation revealed that the SF hydrogel containing SFL-NT3 exhibited a more stable release profile than the SF hydrogel containing NT3 (Fig. 1D b). Moreover, the 5 % SF hydrogel did not adversely affect cell viability or proliferative capacity compared with the control group (Fig. S1). We also evaluated FTIR spectra. The results showed significant absorption peaks of NT3 recombinant protein, SF hydrogel and SF + SFL-NT3 hydrogel. A characteristic peak at 997.71973 cm^{-1} of NT3 recombinant protein appeared in the spectrum of the SF + SFL-NT3 hydrogel, which proves that SFL-NT3 is successfully bound to the hydrogel chain (Fig. S2). Finally, we examined the mechanical properties of silk fibro-based hydrogels. 1 % and 5 %SF showed similar storage moduli (Fig. S3).

3.2. SF + SFL-NT3 hydrogel accelerates wound healing in mice

To assess whether SF + SFL-NT3 accelerated wound healing *in vivo*, a mouse model of full-thickness skin wound injury was used, with PBS, SF, or SF + SFL-NT3 applied every three days. A wound measuring 1 cm in diameter was created on the back of each mouse (Fig. 2A). No mortality

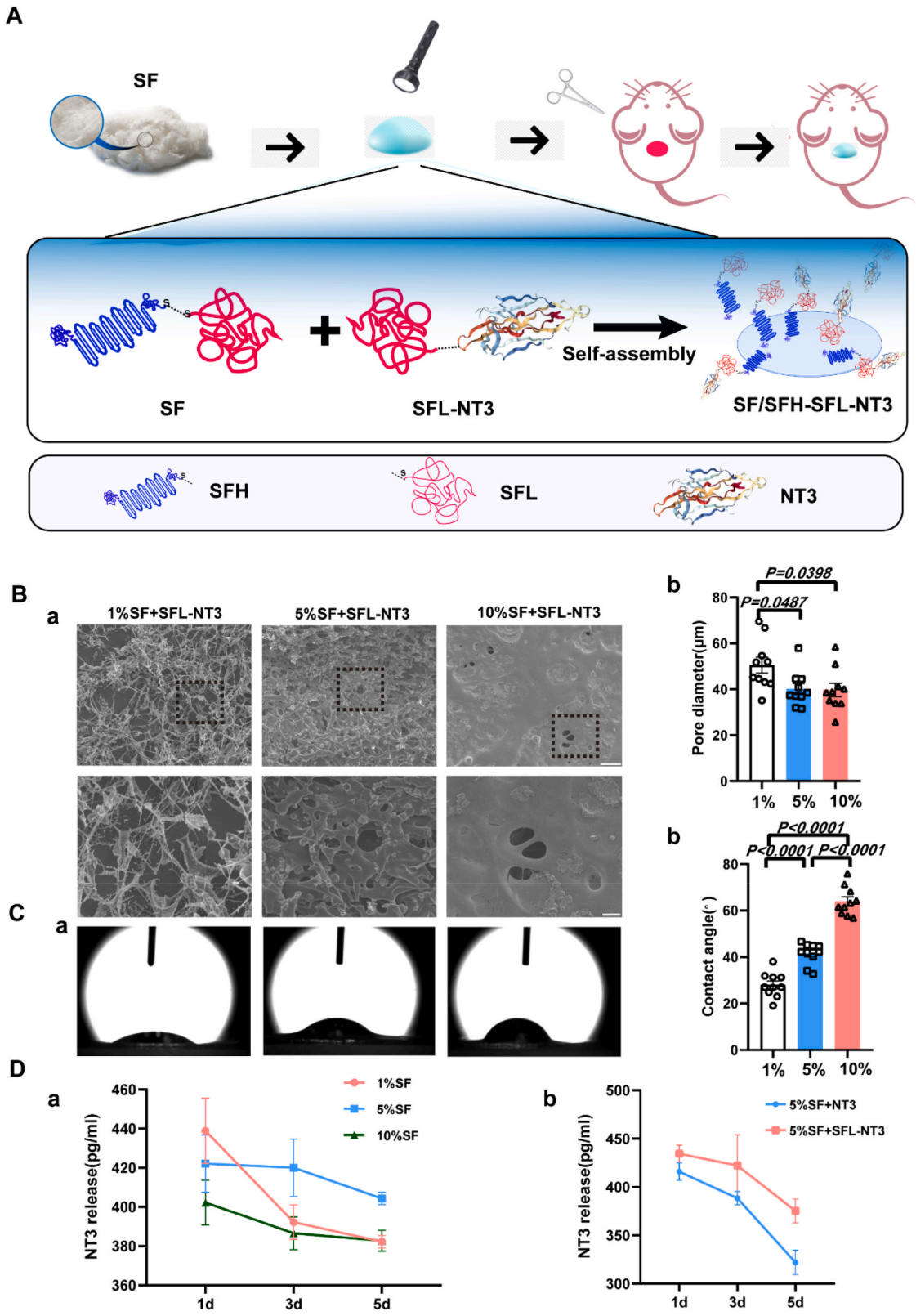

Fig. 1. Fabrication and characterization of the SF + SFL-NT3 hydrogel. (A) The schematic diagram of SF + SFL-NT3 hydrogel preparation and its application in wound healing model. (B, a-b) The SEM photographs of SF + SFL-NT3 and the pore size analysis of hydrogels with different concentration, scale bar = 100 μm and 500 μm. Pore size analysis of the SF + SFL-NT3 hydrogel (n = 10). (C, a-b) Water contact angles of the SF + SFL-NT3 hydrogel with different concentration. Water contact angles analysis of the SF + SFL-NT3 hydrogel (n = 10). (D, a) NT3 release profile from the SF + SFL-NT3 hydrogel in PBS at different SF concentrations over 5 days (n = 3). (D, b) NT3 release profile from the SF + NT3 hydrogel and SF + SFL-NT3 hydrogel in PBS over 5 days (n = 3). Data were analyzed using one-way ANOVA followed by Tukey's post hoc test. *P*-values are presented in the figure. Statistical significance was set at $P < 0.05$.

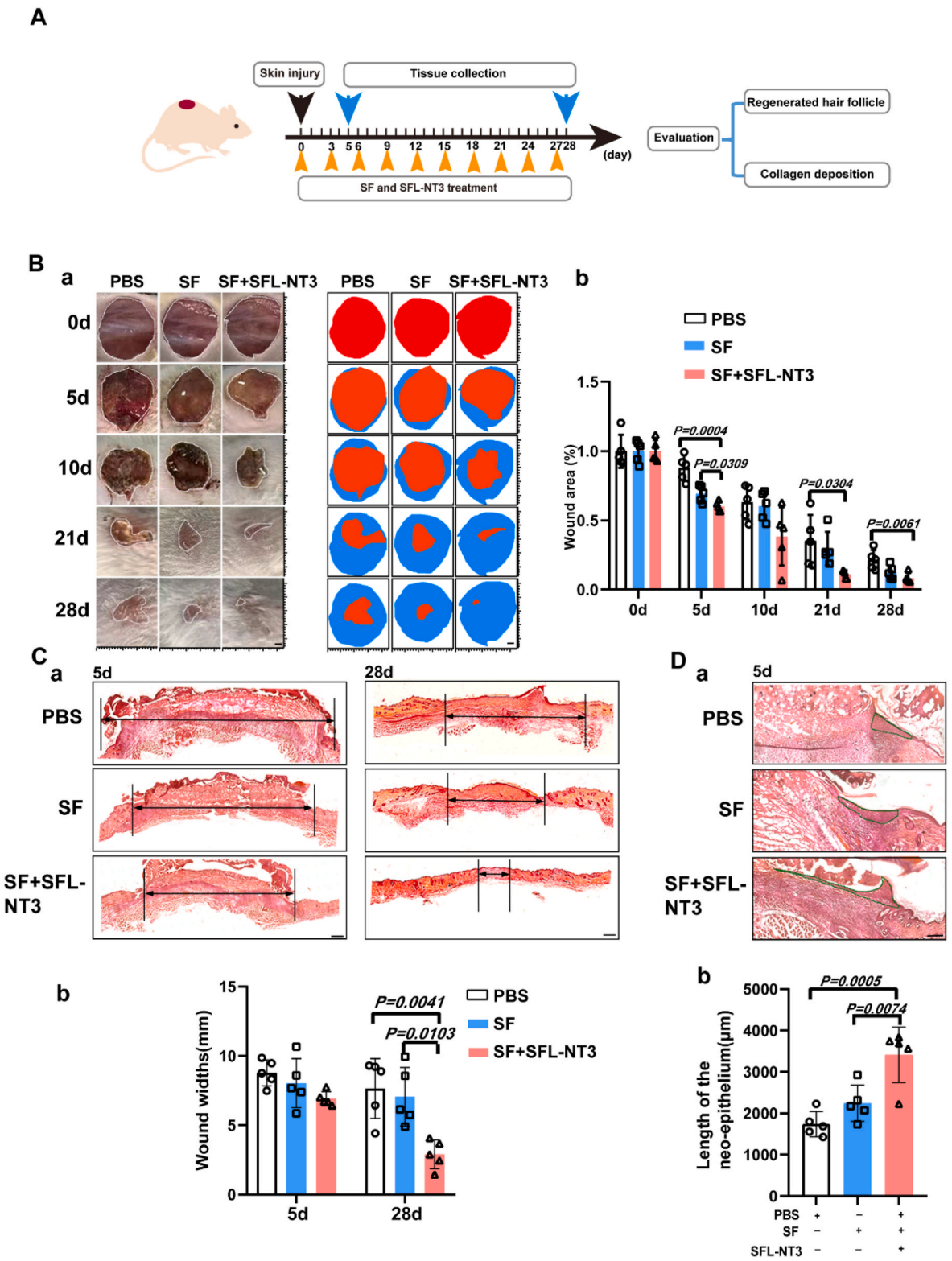

Fig. 2. SF + SFL-NT3 hydrogel promoted full-thickness wound healing in mice. (A) Schematic diagram illustrating the skin wound model and hydrogel treatment in mice. (B, a) Representative images of the wound area at days 0, 5, 10, 21, and 28 after injury in hydrogel-treated mice. (B, b) Statistical analysis of the wound area ratios for skin treated with different materials (n = 5 mice). (C, a-b) Representative images and statistical analysis of wound healing in PBS, SF, and SF + SFL-NT3-treated groups (n = 5 mice). Scale bar = 1 mm. (D, a-b) Representative images and statistical analysis of epithelial tongue length in treated wounds (n = 5 mice). Scale bar = 500 μm. Data were analyzed using one-way ANOVA followed by Tukey's post hoc test. Statistical significance was set at $P < 0.05$.

or abnormalities were observed after surgery. The initial wound sizes in the four groups were almost identical on the first day. By day 5, the wound area in the PBS control group had reduced by 87.9 %, whereas that in the SF group had reduced by 75.2 %. The SF + SFL-NT3 group exhibited the best healing, with a wound area reduction of 60.1 %, which was significantly lower than that in the PBS group. On day 10, the wounds in all groups scabbed and contracted noticeably, with the SF + SFL-NT3 group showing the most advanced healing and the smallest wound area. On days 21 and 28, wound recovery in the SF + SFL-NT3 group remained superior, further indicating its role in promoting faster wound closure (Fig. 2B a, b). Histological analysis *via* H&E staining confirmed the wound area measurements and showed consistent results (Fig. 2C a, b). Re-epithelialization, which is essential for wound healing, was assessed on day 5 by evaluating the length of the epithelial tongue. The SF + SFL-NT3 hydrogel group demonstrated superior re-epithelialization compared with the PBS and SF groups (Fig. 2D a, b). Innervation is critical for epimorphic regeneration such as in the limbs of axolotls [17,20]. Previous studies using chicken and mouse models have shown delayed or impaired wound healing in denervated tissues [21,22]. We investigated whether the innervation of the wound site was enhanced in the SFL-NT3 group. Then we quantified the fluorescence intensity of Tuj1 in immunostaining assay, and demonstrated that the relative fluorescence intensity of Tuj1 in PBS group, SF group and SF + SFL-NT3 group were 1 ± 0.4 (normalized), 1.017 ± 0.23 and 3.566 ± 1.1 respectively (Fig. S4). These results indicated that the SF + SFL-NT3 hydrogel enhanced both innervation and re-epithelialization of the wound tissue.

The effect of SFL-NT3 on the expression of other growth factors at the wound site was also investigated. As key hubs of peripheral sensory afferents, the axons of DRG neurons directly extend within the skin to form a sensory nerve terminal network, constituting the anatomical basis of cutaneous nerve innervation and orchestrating the physiological and pathological functions of cutaneous cell [23]. Moreover, NT3 is a key neurotrophic factor that targets and regulates the survival of DRG neurons and axon regeneration [24]. Therefore, we evaluated factor levels in cultured DRG neurons treated with SFL-NT3. Given the proposed role of NT3 in modulating neuronal cells, factor levels in cultured DRG neurons treated with SFL-NT3 were assessed. The results demonstrated that SFL-NT3 upregulated the expression of FGF1, FGF2, FGF7, FGF8, FGF9, FGF10, and NGF in these neurons (Fig. S5A). Fibroblast growth factors (FGFs) are critical for wound healing [25], while NGF contributes to reduced healing time and improved scar quality [26]. We confirmed the effect of SFL-NT3 on NGF levels *in vivo* and found that NGF expression was increased by SF + SFL-NT3 treatment 5 d after skin tissue injury (Fig. S5B).

The effect of NT3 on angiogenesis was also evaluated. Blood vessels play a vital role in supplying nutrients, oxygen, and growth factors essential for tissue regeneration, as well as in releasing paracrine signals that regulate cellular growth, differentiation, and repair. HE staining revealed a significant increase in the vascular area in the SFL-NT3-treated group (Fig. S6). These data indicate that SFL-NT3 induces the expression of other growth factors and improves innervation and vascularization in the regenerated tissue, which might contribute to a better outcome after injury.

3.3. SF + SFL-NT3 hydrogel promotes the synthesis of Col3 and hair follicle formation

Collagen in the normal skin primarily consists of type I and type III collagen, and the ratio of type III to type I collagen plays a critical role in scar formation [27]. Previous studies have shown that fetal wound healing occurs without scarring, which is attributed to a higher proportion of type III collagen [28]. Collagen deposition in each group was assessed by Masson's trichrome staining. The results indicated that the SF + SFL-NT3 group exhibited 1.8 times more collagen deposition than the PBS group on day 5 after skin injury (Fig. 3A). The formation of skin appendages, such as hair follicles, is a hallmark of regenerative healing [29]. Hair follicle formation during wound healing, with or without NT3 treatment, was evaluated by HE staining. On day 5, the SF + SFL-NT3 group showed three times more new hair follicles than the PBS group, and the SF group displayed more hair follicles than the control group (Fig. 3B, a, c). By day 28, the SF + SFL-NT3 group showed the highest number of new hair follicles (Fig. 3B, b, d). Unexpectedly, SFL-NT3 significantly increased the expression of type III collagen, but had no effect on type I collagen expression in cultured cells (Fig. S7). A similar pattern was observed in a skin injury model. We validated the effects of SF + SFL-NT3 on Col1 and Col3 expression *in vivo* using immunofluorescence staining. The results showed that There was no significant difference in Col1 levels among the groups (Fig. 3C, a, b), but the Col3 level in the SF + SFL-NT3 group was 2.5 times higher than that in the PBS group (normalized to 1). The Col3 level of SF group was slightly higher than that in the control group (Fig. 3C, c, d). Furthermore, as shown in Fig. 3 D, compared to the PBS group, SF + SFL-NT3 treatment resulted in 2-fold increase in Col3 protein levels, but Col1 protein expression remained unchanged in skin tissue that had been injured for 5 days. Therefore, we proved that SF + SFL-NT3 induced a high collagen III/I ratio, which is consistent with data showing that SF + SFL-NT3 promotes wound healing.

3.4. Single cell data analysis of skin fibroblast responded to NT3 treatment

Collagen in the skin is primarily synthesized by fibroblasts. Therefore, the expression of NT3 receptor, tyrosine kinase receptor C (TrkC) and P75, also known as TNF receptor superfamily member 1 B (TNFRSF1B), was investigated in skin fibroblasts. The scRNA-seq data from a previous study (GEO: GSE 142471) [30], which included normal and day-4 post injury mouse skin samples, were reanalyzed. P75 expression was not observed among the differentially expressed genes; therefore, TrkC expression was examined further. The cell types were annotated according to the different markers that have been reported, as well as gene expression profiles. Clustering algorithms and gene enrichment analyses were used to cluster and group cells. The cells are divided into seven distinct types: endothelial cells, HF-associated cells, fibroblasts, epidermal basal cells, spinous cells, dendritic cells, and T cells. These types were further subdivided into 27 clusters (0–26) based on their gene expression profiles (Fig. 4A a, b, Table S1). The results revealed that Col3 was among the top ten differentially expressed genes in cluster 4, which also exhibited elevated TrkC expression in cluster 4 fibroblasts (Fig. 4A c, d). Cluster 4 also expressed other reticular fibroblast markers including Mfap5, Gpc3, Fbn1, CD34, and Lum [31]. Reticular fibroblasts secrete substantial amounts of collagen and extracellular matrix and are critical for wound healing. In addition, Col3 secreted by reticular fibroblasts plays a pivotal role in the regeneration of mouse fingertips [28]. Fig. 3C and D demonstrate that SF + SFL-NT3 hydrogel treatment promoted Col3 expression, suggesting that it may also stimulate Col3 production in reticular fibroblasts, thereby aiding wound healing. To explore the expression patterns of TrkC and Col3 *in vivo*, immunofluorescence staining was performed, which revealed that TrkC colocalized with Col3 in regenerated skin treated with NT3 (Fig. 4B a, b). This result suggested that NT3 could activate TrkC in fibroblasts at sites of regeneration in skin lesions, and that activation of TrkC increased Col3 expression and promoted scarless wound recovery.

3.5. SFL-NT3 increases Col3 expression via upregulating Sox2 level in fibroblast

Upon treatment with SFL-NT3, L929 cells exhibited a significant increase in both the protein expression (Fig. 5A) and immunofluorescence intensity of Col3 (Fig. 5B), whereas the protein expression of Col1 remained unchanged. To elucidate the signaling pathways mediating the effect of SFL-NT3 on Col3 expression, L929 cells were used as an *in*

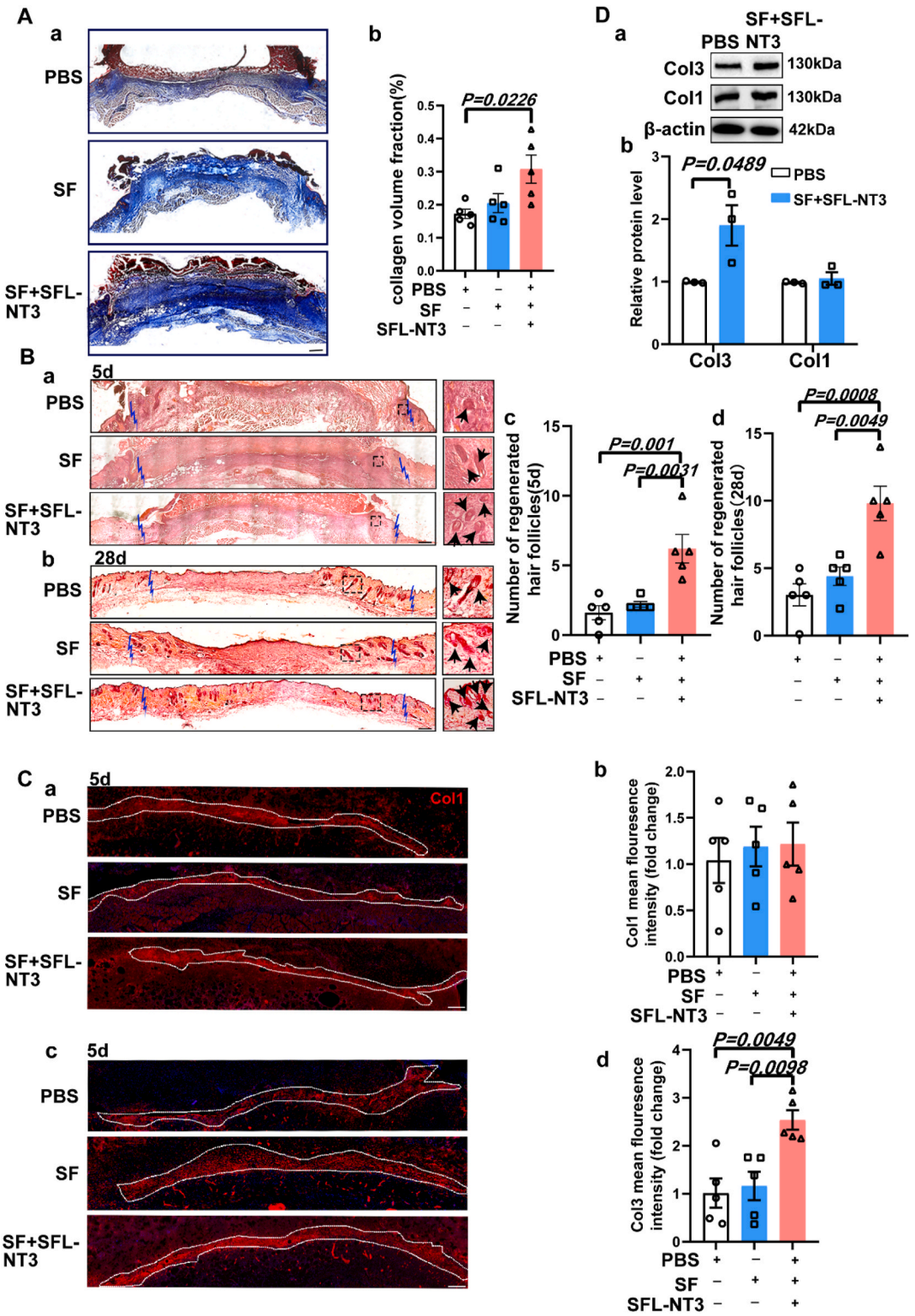

Fig. 3. SF + SFL-NT3 promotes the synthesis of Col3 and accelerates hair follicle regeneration in mice. (A, a) Masson's Trichrome staining to visualize collagen deposition in tissue samples from PBS, SF, and SF + SFL-NT3 groups. Scale bar = 500 μm. (A, b) Quantitative analysis of collagen deposition by Masson's Trichrome staining. Data are expressed as means ± SE (n = 5 mice). (B, a-b) Representative H&E images of skin sections from PBS, SF, and SF + SFL-NT3 groups on days 5 and 28. Enlarged views of the boxed areas are shown on the right. Scale bars = 500 μm (left panel) and 200 μm (right panel). The blue lightning area indicates the initial damage zone. (B, c-d) Statistical analysis of regenerated hair follicles at the wound site. Data are expressed as means ± SE (n = 5 mice). (C, a) Representative immunofluorescence staining images showing Col1 (red) and DAPI (blue) in skin sections. Scale bar = 500 μm. (C, b) Statistical analysis of average fluorescence intensity of Col1. Data are expressed as means ± SE (n = 5 mice). (C, c) Representative immunofluorescence staining images of Col3 (red) and DAPI (blue) in skin sections. Scale bar = 500 μm. (C, d) Statistical analysis of average fluorescence intensity of Col3. Data are presented as mean ± SE (n = 5 mice). (D, a-b) Western blotting analysis of Col3 and Col1 expression in skin wounds treated with PBS and SF + SFL-NT3 hydrogel. β-actin was used as a control. Data are presented as means ± SE (n = 3). Data were analyzed using Student's *t*-test and one-way ANOVA followed by Tukey's post hoc test. *P*-values are presented in the figure. Statistical significance was set at $P < 0.05$. (For interpretation of the references to color in this figure legend, the reader is referred to the Web version of this article.)

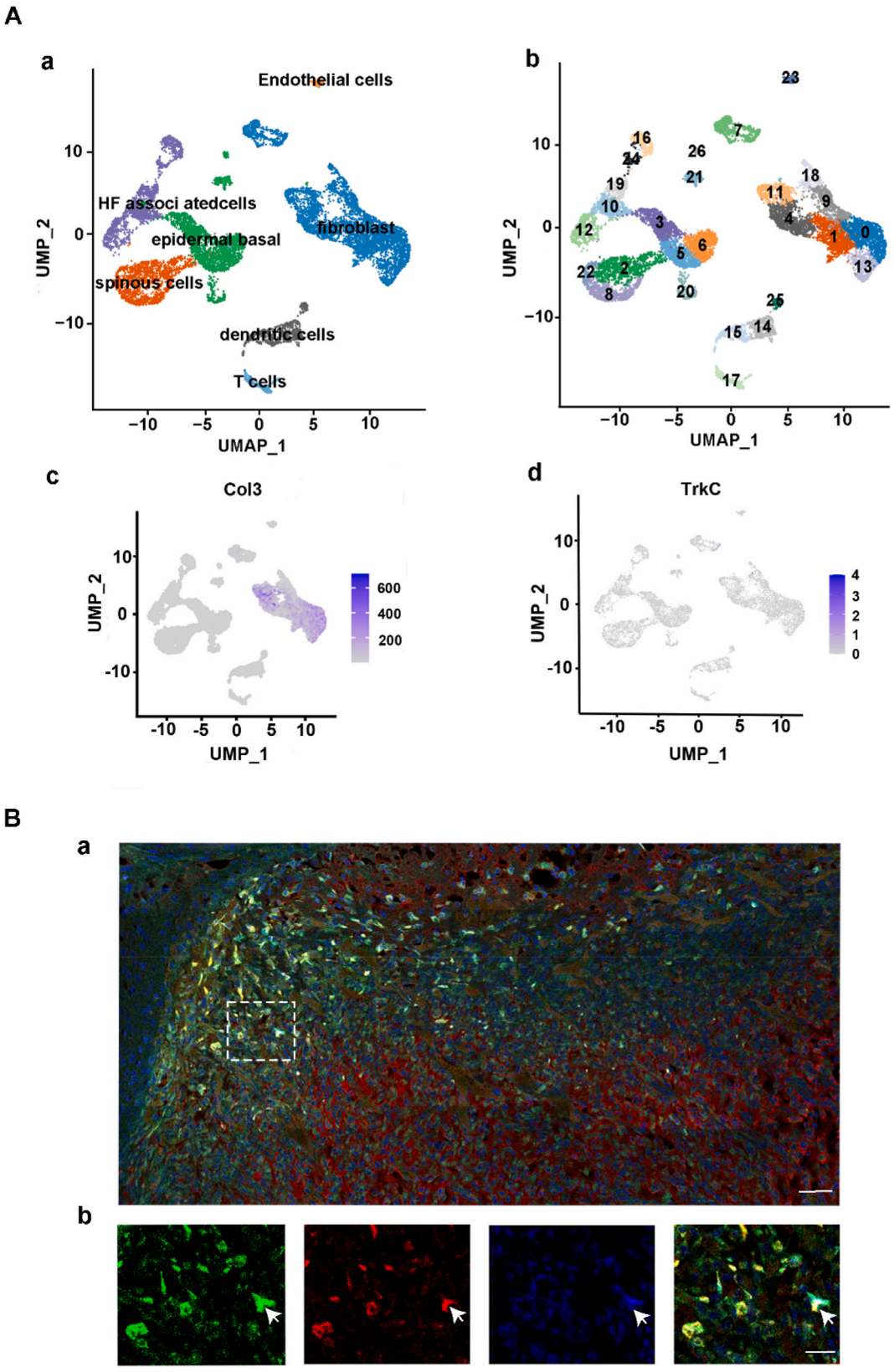

Fig. 4. Single-cell data analysis of skin fibroblasts. (A, a-b) UAMP plots colored by cell type from single-cell sequencing, where each dot represents an individual cell and different colors indicate different cell taxa. (A, c) Relative expression of Col3 across various cell types. (A, d) Expression of TrkC across various cell types. (B, a-b) Representative immunofluorescence staining images of skin sections from the back of mice in the SF + SFL-NT3 group. Arrows indicate co-labeled cells. Red indicates Col3, green indicates TrkC, and blue indicates DAPI. Scale bars = 500 μm (upper panel) and 200 μm (lower magnified panel). (For interpretation of the references to color in this figure legend, the reader is referred to the Web version of this article.)

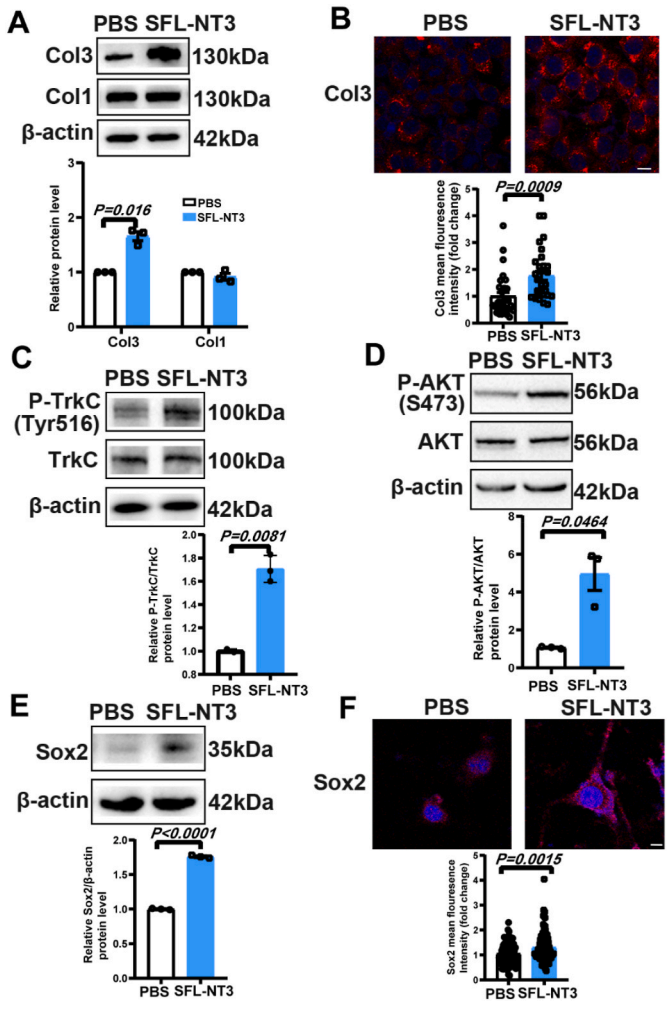

Fig. 5. SFL-NT3 regulates Col3 expression through activation of the TrkC/Akt/Sox2 pathway. (A). Representative Western blotting and statistical analysis of Col3 and Col1 expression after L929 cells were treated with SFL-NT3 recombinant protein. Col3 and Col1 values in the PBS group were normalized to 1. (n = 3) (B) Representative images and statistical analysis of immunofluorescence staining in L929 cells. Red indicates Col3. Scale bars = 10 μm. (n = 30; experiment repeated 3 times). (C) Representative Western blotting and statistical analysis of P-TrkC expression after L929 cells were treated with SFL-NT3 recombinant protein. P-TrkC values in the PBS group were normalized to 1. (n = 3) (D) Representative Western blotting and statistical analysis of P-Akt and Akt expression after L929 cells were treated with SFL-NT3 recombinant protein. P-Akt and Akt values in the PBS group were normalized to 1. (n = 3) (E) Representative Western blotting and statistical analysis of Sox2 expression after L929 cells were treated with SFL-NT3 recombinant protein. Sox2 values in the PBS group were normalized to 1. (F) Representative images and statistical analysis of immunofluorescence staining in L929 cells. Red indicates Sox2, and blue indicates DAPI. Scale bars = 10 μm. (n = 90; experiment repeated 3 times). Data are presented as mean ± SE. Statistical analysis was performed using Student's *t*-test. Data were analyzed using Student's *t*-test. *P*-values are presented in the figure. Statistical significance was set at $P < 0.05$. (For interpretation of the references to color in this figure legend, the reader is referred to the Web version of this article.)

vitro model to assess the activation of potential signaling molecules, including TrkC, an NT3 receptor. Results indicated that SFL-NT3 treatment notably enhanced TrkC phosphorylation (at Tyr516), confirming TrkC activation (Fig. 5C). The Akt pathway, which regulates critical cellular processes, such as survival, growth, proliferation, angiogenesis, metabolism, and migration [32], was also evaluated. Phosphorylation of Akt (S473) was markedly increased in L929 cells treated with SFL-SFL-NT3, as shown in Fig. 5D, which aligns with previous research [33]. To further reveal the pathway responsible for the increased transcription of Col3 upon SFL-NT3 treatment, we predicted the possible transcription factors that might bind to the Col3 promoter sequence and identified transcription factors that could also be regulated by Akt activation. We found Sox2 is a candidate transcription factor that modulate Col3 expression. Therefore, we evaluated the effect of SFL-NT3 on the expression of Sox2 in L929 cells. Results revealed that SFL-NT3 treatment significantly elevated Sox2 protein expression and increased Sox2 immunofluorescence intensity, consistent with previous findings [34] (Fig. 5E and F).

Using the Jaspar database, Sox2 binding sites in the Col3 promoter sequence were predicted (Fig. 6A–a), and plasmids containing the Col3 promoter region and Sox2 core sequence were constructed for luciferase reporter assays. The results demonstrated that Sox2 significantly enhanced Col3 transcription (Fig. 6A and b). ChIP assays further confirmed Sox2 enrichment in the Col3 promoter region compared to the IgG control group (Fig. 6B–a). Gel electrophoresis of the qRT-PCR products showed that the density of Sox2 bands was greater than that of the IgG control group (Fig. 6B–b). These results suggest that Sox2 positively regulates Col3 expression.

MK2206 is an orally active, blood-brain barrier permeable Akt inhibitor, and MK2206 significantly reduced Sox2 and Col3 expression (Fig. 6C). When Sox2 was knock down by siRNA in L929 as showed in Fig. S8, the increased expression of Col3 protein via SFL-NT3 treatment was also significantly reduced (Fig. 6D). These results indicated that SFL-NT3 dependent activation of TrkC activates the AKT pathway, further increasing Sox2 levels and enhancing Col3 expression.

3.6. *TrkC inhibitor inhibits Col3 synthesis in vivo*

To further validate the effect of NT3 on Col3 levels, a Trk inhibitor was applied to a mouse model of back skin injury to determine whether LPM4870108, a potent and orally active Trk inhibitor, inhibited the upregulation of Col3 expression induced by SFL-NT3 treatment. A schematic diagram of the experimental setup is shown in Fig. 7A. On day 5 post-injury, the healing rate in the SF + SFL-NT3 group was significantly higher than that in the control group, whereas the healing rate in the SF + SFL-NT3+LPM4870108 group was comparable to that in the control group (Fig. 7B–a, b). These findings suggest that TrkC inhibition impairs wound healing in mice. Histological analysis using H&E staining further supported this finding, showing that on day 5, the number of regenerated hair follicles in the SF + SFL-NT3+LPM4870108 group was only half that in the SF + SFL-NT3 group, resembling the pattern observed in the PBS group (Fig. 7C–a, b). Similarly, a TrkC inhibitor decreased collagen synthesis. The results showed that on the 5th day after skin injury, the collagen deposition in the SF + SFL-NT3 group was higher than that in the PBS group. However, after the addition of the inhibitor LPM4870108, the proportion of collagen deposition decreased (Fig. S9). Further experiments showed that the quantity of Col1 did not vary among the groups, whereas that of Col3 in the SF + SFL-NT3 group was significantly higher than that in the SF + SFL-NT3+LPM4870108 group, which was similar to that in the control group (Fig. 7D and E). Based on these results, NT3 treatment effectively facilitated hair follicle regeneration and Col3 synthesis at the wound site.

4. Conclusion

In this study, a novel skin repair system based on SF materials combined with NT3 was developed, which significantly improved the sustained-release performance of NT3 through material optimization. The results showed that the SF + SFL-NT3 hydrogel promoted rapid skin healing and hair follicle regeneration. NT3 exhibits a new effect beyond traditional neurotrophic functions in skin repair; it achieves scar-free repair by activating the Akt signaling pathway and upregulating the expression of the transcription factor Sox2, thereby selectively promoting the synthesis of Col3 rather than Col1 (Fig. 8). Our research

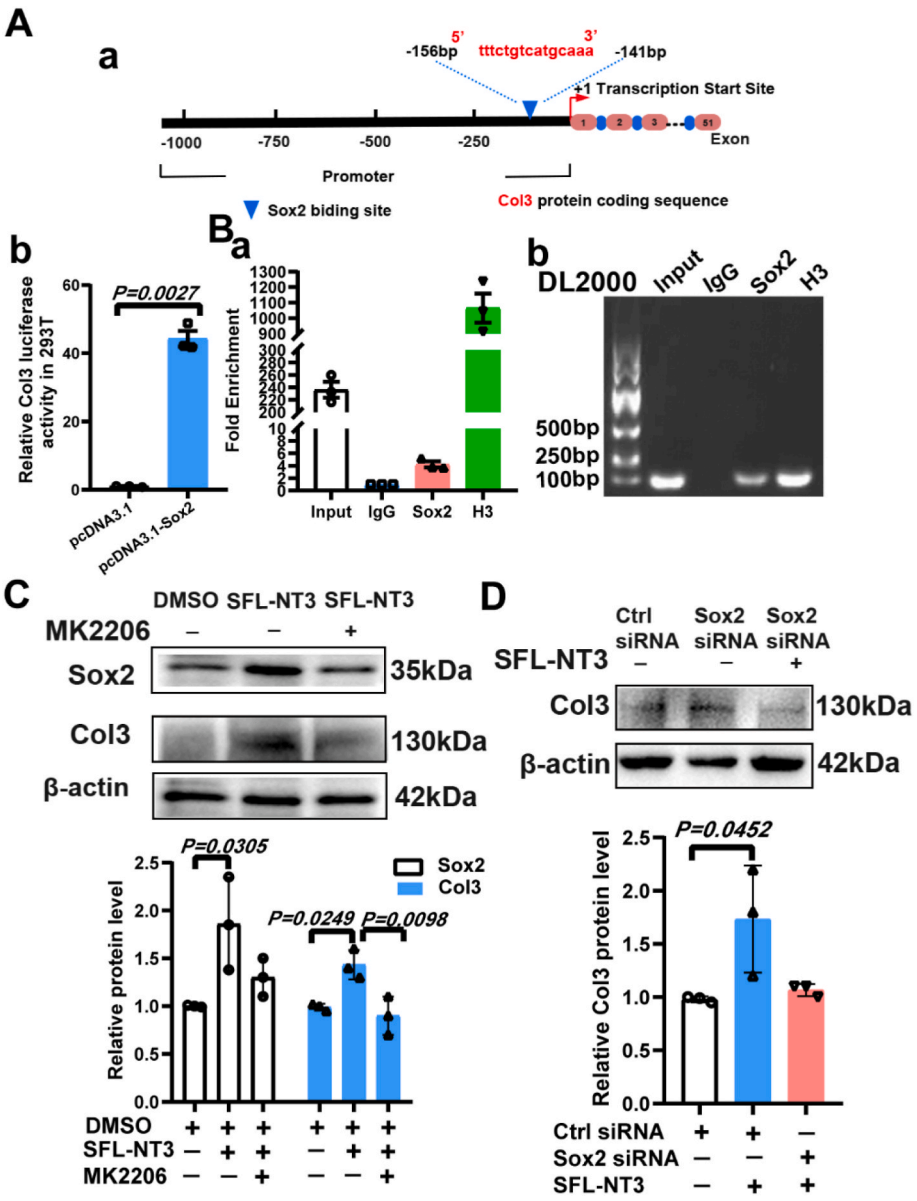

Fig. 6. Sox2 positively regulates Col3 expression. (A, a) The Jaspar database predicted Sox2, a transcription factor, to bind the Col3 gene *via* a specific binding site. (A, b) HEK-293T cells were transfected with either the Col3 promoter plasmid or the Col3 promoter plasmid along with pcDNA3.1-Sox2 for 48 h. Statistical analysis was performed using Student's *t*-test. Data are presented as the means ± SE (n = 3). (B, a) ChIP analysis demonstrated Sox2 enrichment in the Col3 promoter region, compared to the IgG promoter region. (B, b) Gel electrophoresis of qRT-PCR products showed Sox2 grayscale values exceeding those of IgG (n = 3). (C) Representative Western blotting and statistical analysis of Sox2 and Col3 levels following treatment of L929 cells with SFL-NT3 recombinant protein and the AKT inhibitor MK2206. β-actin served as the loading control. Sox2 and Col3 values in the DMSO-treated group were normalized to 1. Data are expressed as the means ± SE (n = 3). *P*-values are presented in the figure. (D) Representative Western blotting and statistical analysis of Col3 expression following Sox2 siRNA treatment in L929 cells. β-actin was used as the control. Col3 values in the Ctrl siRNA group were normalized to 1. Data are presented as mean ± SE (n = 3). *P*-values are presented in the figure. Data were analyzed using Student's *t*-test and one-way ANOVA followed by Tukey's post hoc test. Statistical significance was set at $P < 0.05$.

offers the prospect of a novel biomaterial, the SF light chain, combined with NT3 for the repair of skin damage, and provides new approach for the design of silk fibroin based biomaterials.

5. Discussion

Adult skin wound healing often leads to scar formation accompanied by severe pain and impaired mobility. Various wound-dressing materials and skin substitutes have been developed to achieve scar-free or scarless healing. SF has been extensively studied in tissue engineering owing to its excellent biocompatibility, low number of inflammatory reactants, and ease of processing [35]. SF-based hydrogels have a highly porous structure that functions as an extracellular matrix (ECM) mimic, providing a suitable environment for cell growth, and injectable hydrogels can re-expand to the desired shape according to defect [36]. In this study, an SF-based hydrogel combined with recombinant NT3 was designed to promote the healing of full-thickness skin injuries. The results demonstrated that the wound dressing significantly accelerated the healing process and reduced scar tissue formation, thereby providing an effective approach for skin injury treatment.

Silk firoin based material show many excellent properties as a dressing for skin repair. The hydrophilicity of SF hydrogels is conducive to the absorption of wound exudate [37] and the adsorption of proteins on the wound surface [38]. There are dynamic crosslinking sites in the hydrogel network that allow the hydrogel network to flow under stress, enabling cells to enrich adhesion sites and promote focal adhesion

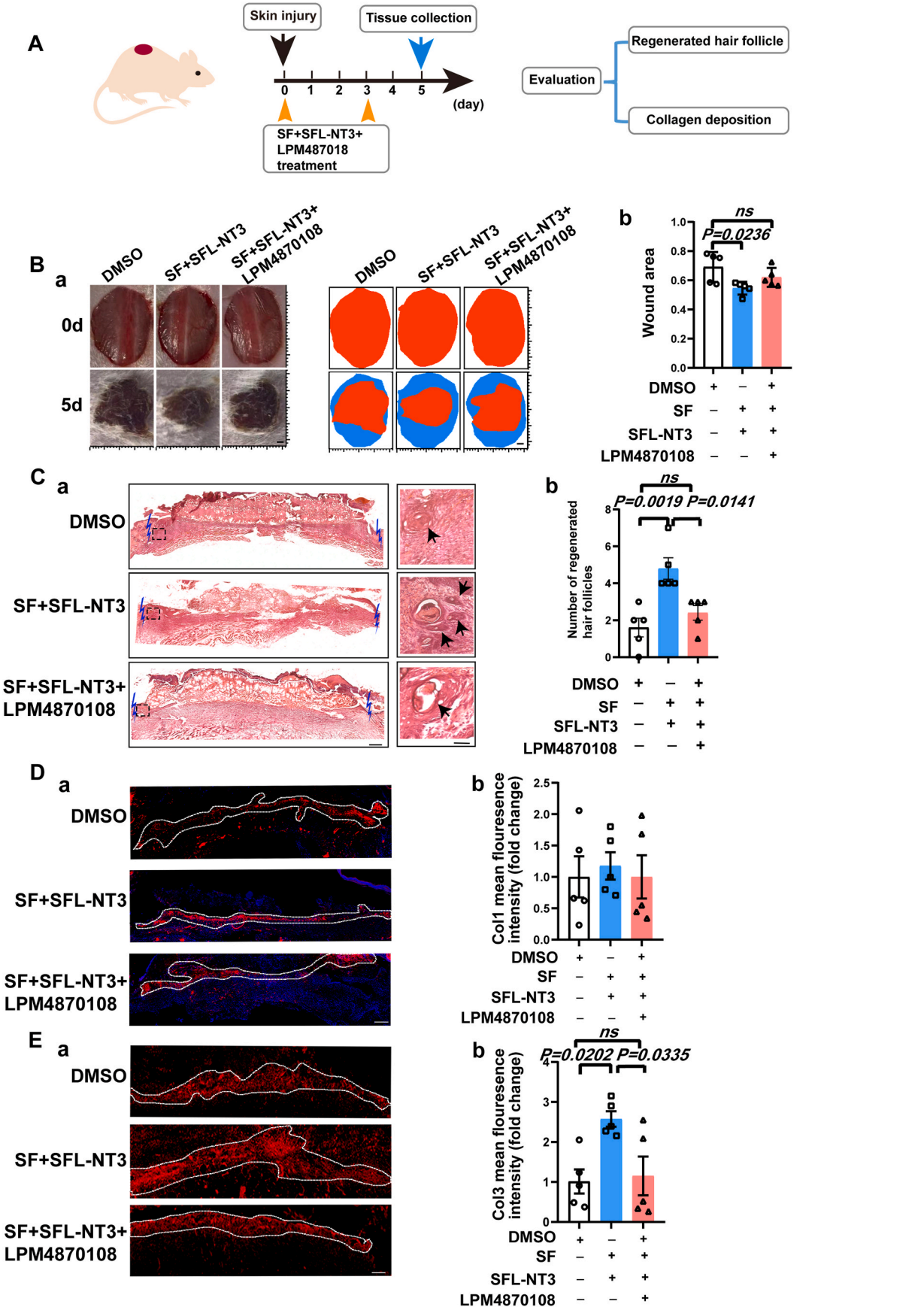

(caption on next page)

Fig. 7. TrkC inhibitors suppress Col3 synthesis *in vivo*. (A) Schematic representation of skin wound and hydrogel treatment protocols. (B, a) Representative images of wound areas following different treatments on days 0 and 5 post-injury. (B, b) Wound area ratios at different time points for treatments with various materials (n = 5 mice). (C, a) Representative HE staining images of skin sections from DMSO, SF + SFL-NT3, and SF + SFL-NT3+LPM4870108 groups. Enlarged regions are shown on the right. Scale bars = 500 μm (left panel) and 200 μm (right panel). (C, b) Statistical analysis of regenerated hair follicles at the wound site. Data are presented as means ± SE (n = 5). (D, a) Representative immunofluorescence images of skin sections. Red indicates Col1, and blue indicates DAPI. Scale bars = 500 μm. (D, b) Statistical analysis of average fluorescence intensity of Col1. Data are expressed as means ± SE (n = 5). (E, a) Representative immunofluorescence staining images of skin sections from the back of mice. Red indicates Col3, and blue indicates DAPI. Scale bars = 500 μm. (E, b) Statistical analysis of the average fluorescence intensity of Col3. Data are expressed as mean ± SE (n = 5). Data were analyzed using one-way ANOVA followed by Tukey's post hoc test. *P*-values are presented in the figure. Statistical significance was set at $P < 0.05$. (For interpretation of the references to color in this figure legend, the reader is referred to the Web version of this article.)

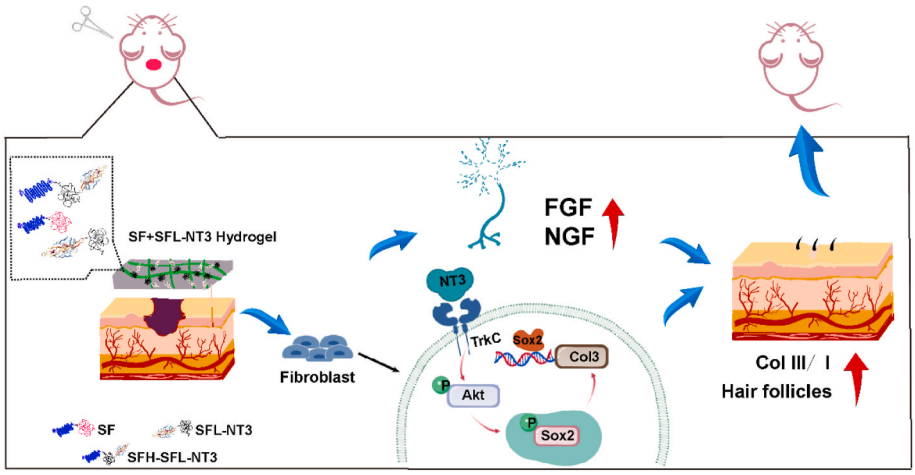

Fig. 8. Schematic illustration of SF + SFL-NT3 hydrogel production and its application in promoting scarless skin injury recovery. The SF + SFL-NT3 hydrogel is self-assembled from SF and SFL-NT3 to form SFH-SFL-NT3. This hydrogel material enhances skin repair with minimal scarring by stimulating neuronal axon growth and type III collagen deposition in fibroblasts.

maturation, thereby promoting cell-related pathways, cell adhesion, and related differentiation [39]. Regarding the selection of a 5 % SF concentration, although its sustained-release property is beneficial for the continuous action of NT3, its lower mechanical strength may limit its application to dynamic wounds (such as joint areas). In the future, gradient cross-linking technology or a combination with other biopolymers should be developed to balance mechanical properties and biological activity. These studies provide a key theoretical basis and technical support for the development of precise, clinically translatable, scarless repair materials.

Wound dressings that incorporate bioactive growth factors can significantly enhance therapeutic outcomes. These factors can be integrated into dressing materials *via* adsorption, carrier entrapment, or covalent attachment. Adsorption refers to the decoration of silk surfaces with proteins by weak forces such as van der Waals forces or hydrophobic interactions. Although adsorption is advantageous owing to its ease of processing and cost-effectiveness, it suffers from low retention and susceptibility to degradation. In the present study, an SF-based hydrogel containing NT3 was designed, in which NT3 was fused with the light chain of SF, which was linked to the heavy chain through disulfide bonds. This approach allowed the efficient integration of NT3 into the hydrogel, while retaining the benefits of entrapment or covalent attachment. Recombinant silk proteins may serve as favorable biomaterials for various SF-based tissue-engineering products. In addition, recombinant proteins can incorporate diverse factors that cater to the specific needs of different clinical treatments.

The release of growth factors and cytokines at wound sites is essential for effective skin healing. Numerous studies have demonstrated the advantages of the local delivery of growth factors to enhance wound repair [40]. It is well known that NT3 is a neurotrophic factor with multiple functions in the peripheral and central nervous systems in development and regeneration. Considering that innervation is critical for wound healing, we tested the effect of NT3 on nerve growth at the wound site and found that NT3 significantly improved tissue innervation, and subsequently facilitated the recovery of skin wounds. Surprisingly, exogenous NT3 had an additional effect on matrix deposition, which significantly contributed to wound healing. SF hydrogel containing SFL-NT3 resulted in less scar skin healing in a model of full-thickness injury to mouse skin by promoting the deposition of Col3. Col3 is a fibrillary collagen present during embryonic development and wound healing [41]. Col1 serves as the primary structural component of fibers, whereas Col3 regulates fiber diameter and growth during fiber formation [42]. Mutations in Col3 are associated with Ehler–Danlos syndrome IV, in which skin wounds heal with excessive scarring [43]. Elevated Col3 levels in scarless fetal wounds and a mouse fingertip regeneration model [44] further support its role in promoting minimal scar skin regeneration. Therefore, Col3 plays a beneficial role in reducing scar skin regeneration [45]. This study highlights the effects and mechanisms by which SFL-NT3 enhances matrix deposition in fibroblasts, thereby providing a novel strategy for wound healing.

Although the SF + SFL-NT3 hydrogel developed in this study shows the potential for promoting scarless healing in animal models, its clinical translation still needs to overcome multiple biological and engineering challenges. First, the fibroblast differentiation process during human skin healing (such as fibroblast differentiation maturity, skin layer-specific differentiation time windows, and differentiation kinetics driven by pregnancy cycles) differs significantly from that in mice [46]. Therefore, it is necessary to systematically evaluate the ability of the hydrogel to regulate the Col3/Col1 ratio in human dermal fibroblasts and verify its long-term repair effect and safety in large animal models, such as pigs. Second, the dynamic balance of Col3 has a bidirectional regulatory risk of scar formation; overexpression may lead to a decrease in tissue mechanical strength, whereas insufficient expression may attenuate its inhibitory effect on the thickening of Col1 fibers [47]. Therefore, it is necessary to elaborately regulate the levels of Col1 and Col3 taking account the related pathways such as Sox2 [48], TGF-β/Smad3 [49,50], and Hippo-YAP [51].

Based on the successful paradigm of SF light chain and NT3, this

technology can construct a multi-factor collaborative composite repair system - for example, by anchored VEGF dimer and TGF-β dimer to SF scaffolds to simultaneously drive angiogenesis and differentiation, or by tandem NT3 dimer and IL-10 monomer to develop injury repair materials with both nerve regeneration and anti-inflammatory functions. Compared with the residual reagent toxicity and inflammatory response risks that may be caused by the chemical cross-linking method, this material shows better biocompatibility.

In conclusion, we successfully designed a wound dressing based on SF hydrogels, which containing SFL-NT3. This new material has a wide range of potential applications and can be loaded with other factors that promise rapid and minimal scar wound healing.

CRediT authorship contribution statement

Yingying Yan: Writing – review & editing, Writing – original draft, Visualization, Validation, Software, Methodology, Investigation, Formal analysis, Data curation. **Mingxuan Li:** Visualization, Methodology, Data curation. **Longyu Guo:** Methodology, Data curation. **Wenxue Zhang:** Software, Methodology. **Ronghua Wu:** Methodology, Conceptualization. **Tuchen Guan:** Methodology, Conceptualization. **Jue Ling:** Data curation. **Yumin Yang:** Supervision, Conceptualization. **Mei Liu:** Writing – review & editing, Supervision, Funding acquisition, Conceptualization. **Xiaosong Gu:** Funding acquisition, Conceptualization. **Yan Liu:** Writing – review & editing, Writing – original draft, Supervision, Project administration, Investigation, Conceptualization.

Ethics approval

Animals were sourced from the Laboratory Animal Center of Nantong University (Nantong, Jiangsu Province, China). All procedures adhered to the Institutional Animal Care and Use guidelines and National Institutes of Health (Bethesda, MD) guidelines. The study received approval from the Animal Ethics Committee of Nantong University, China.

Funding

National Key R&D Program of China (Grant No. 2024YFA1108200)
The Natural Science Foundation of Jiangsu Province (Grant No. BK20232023)
National Natural Science Foundation of China (Grant No. 32471038)
National Natural Science Foundation of China (Grant No.32070725)
Proof of Concept Projects for Haian Institute of Adanced Textile (No.2025GNYZ005).

Declaration of competing interest

The authors have no competing interests to declare.

Appendix A. Supplementary data

Supplementary data to this article can be found online at https://doi.org/10.1016/j.mtbio.2025.101957.

Data availability

Data will be made available on request.

References

[1] S. Chen, et al., Mechanically and biologically skin-like elastomers for bio-integrated electronics, Nat. Commun. 11 (2020) 1107, https://doi.org/10.1038/s41467-020-14446-2.
[2] Y. Gu, J. Han, C. Jiang, Y. Zhang, Biomarkers, oxidative stress and autophagy in skin aging, Ageing Res. Rev. 59 (2020) 101036, https://doi.org/10.1016/j.arr.2020.101036.
[3] F. Qu, R. Geng, Y. Liu, J. Zhu, Advanced nanocarrier- and microneedle-based transdermal drug delivery strategies for skin diseases treatment, Theranostics 12 (2022) 3372–3406, https://doi.org/10.7150/thno.69999.
[4] P. Martin, Wound healing–aiming for perfect skin regeneration, Science 276 (1997) 75–81, https://doi.org/10.1126/science.276.5309.75.
[5] N.S. Tan, et al., The nuclear hormone receptor peroxisome proliferator-activated receptor beta/delta potentiates cell chemotactism, polarization, and migration, Mol. Cell Biol. 27 (2007) 7161–7175, https://doi.org/10.1128/MCB.00436-07.
[6] D.R. Griffin, et al., Activating an adaptive immune response from a hydrogel scaffold imparts regenerative wound healing, Nat. Mater. 20 (2021) 560–569, https://doi.org/10.1038/s41563-020-00844-w.
[7] Y. Liang, et al., Adhesive hemostatic conducting injectable composite hydrogels with sustained drug release and photothermal antibacterial activity to promote full-thickness skin regeneration during wound healing, Small 15 (2019) e1900046, https://doi.org/10.1002/smll.201900046.
[8] F. Zhou, et al., Rapid printing of bio-inspired 3D tissue constructs for skin regeneration, Biomaterials 258 (2020) 120287, https://doi.org/10.1016/j.biomaterials.2020.120287.
[9] S.P. Zhong, Y.Z. Zhang, C.T. Lim, Tissue scaffolds for skin wound healing and dermal reconstruction, Wiley Interdiscip. Rev. Nanomed. Nanobiotechnol. 2 (2010) 510–525, https://doi.org/10.1002/wnan.100.
[10] S. Mandal, et al., A surfactant-induced functional modulation of a global virulence regulator from Staphylococcus aureus, PLoS One 11 (2016) e0151426, https://doi.org/10.1371/journal.pone.0151426.
[11] W. Zhang, et al., Silk fibroin biomaterial shows safe and effective wound healing in animal models and a randomized controlled clinical trial, Adv. Healthcare Mater. 6 (2017), https://doi.org/10.1002/adhm.201700121.
[12] X.H. Liao, H. Nguyen, Epidermal expression of Lgr6 is dependent on nerve endings and Schwann cells, Exp. Dermatol. 23 (2014) 195–198, https://doi.org/10.1111/exd.12340.
[13] S. Huang, et al., Lgr6 marks epidermal stem cells with a nerve-dependent role in wound re-epithelialization, Cell Stem Cell 28 (2021) 1582–1596.e1586, https://doi.org/10.1016/j.stem.2021.05.007.
[14] K.M. Albers, B.M. Davis, The skin as a neurotrophic organ, Neuroscientist 13 (2007) 371–382, https://doi.org/10.1177/1073858407013040901.
[15] M. Bothwell, Neurotrophin function in skin, J. Invest. Dermatol. Symp. Proc. 2 (1997) 27–30, https://doi.org/10.1038/jidsymp.1997.7.
[16] Y. Yan, et al., Promising application of a novel biomaterial, light chain of silk fibroin combined with NT3, in repairment of rat sciatic nerve defect injury, Int. J. Biol. Macromol. 240 (2023) 124447, https://doi.org/10.1016/j.ijbiomac.2023.124447.
[17] O.A. Pena, P. Martin, Cellular and molecular mechanisms of skin wound healing, Nat. Rev. Mol. Cell Biol. 25 (2024) 599–616, https://doi.org/10.1038/s41580-024-00715-1.
[18] X. Zhu, et al., Foxq1 promotes alveolar epithelial cell death through tle1-mediated inhibition of the NF-kappaB signaling pathway, Am. J. Respir. Cell Mol. Biol. 71 (2024) 53–65, https://doi.org/10.1165/rcmb.2023-0317OC.
[19] R. Wu, et al., Cooperation of long noncoding RNA LOC100909675 and transcriptional regulator CTCF modulates Cdk1 transcript to control astrocyte proliferation, J. Biol. Chem. 299 (2023) 105153, https://doi.org/10.1016/j.jbc.2023.105153.
[20] J.E. Farkas, J.R. Monaghan, A brief history of the study of nerve dependent regeneration, Neurogenesis (Austin) 4 (2017) e1302216, https://doi.org/10.1080/23262133.2017.1302216.
[21] S. Harsum, J.D. Clarke, P. Martin, A reciprocal relationship between cutaneous nerves and repairing skin wounds in the developing chick embryo, Dev. Biol. 238 (2001) 27–39, https://doi.org/10.1006/dbio.2001.0395.
[22] K. Kishi, et al., Mutual dependence of murine fetal cutaneous regeneration and peripheral nerve regeneration, Wound Repair Regen. 14 (2006) 91–99, https://doi.org/10.1111/j.1743-6109.2005.00093.x.
[23] H. Yang, et al., Primary sensory neuron-derived miR-let-7b underlies stress-elicited psoriasis, Brain Behav. Immun. 123 (2025) 997–1010, https://doi.org/10.1016/j.bbi.2024.11.005.
[24] T. Chen, X. He, J. Wang, D. Du, Y. Xu, NT-3 combined with TGF-beta signaling pathway enhance the repair of spinal cord injury by inhibiting glial scar formation and promoting axonal regeneration, Mol. Biotechnol. 66 (2024) 1484–1495, https://doi.org/10.1007/s12033-023-00781-4.
[25] Y. Qu, et al., The dual delivery of KGF and bFGF by collagen membrane to promote skin wound healing, J. Tissue Eng. Regen. Med. 12 (2018) 1508–1518, https://doi.org/10.1002/term.2691.
[26] G.E.B. M, et al., Nerve growth factor and burn wound healing: update of molecular interactions with skin cells, Burns 49 (2023) 989–1002, https://doi.org/10.1016/j.burns.2022.11.001.
[27] R. Riekki, et al., Increased expression of collagen types I and III in human skin as a consequence of radiotherapy, Arch. Dermatol. Res. 294 (2002) 178–184, https://doi.org/10.1007/s00403-002-0306-2.
[28] L. Marrero, J. Simkin, M. Sammarco, K. Muneoka, Fibroblast reticular cells engineer a blastema extracellular network during digit tip regeneration in mice, Regeneration (Oxf) 4 (2017) 69–84, https://doi.org/10.1002/reg2.75.
[29] M. Takeo, W. Lee, M. Ito, Wound healing and skin regeneration, Cold Spring Harb. Perspect. Med. 5 (2015) a023267, https://doi.org/10.1101/cshperspect.a023267.
[30] D. Haensel, et al., Defining epidermal basal cell states during skin homeostasis and wound healing using single-cell transcriptomics, Cell Rep. 30 (2020) 3932–3947 e3936, https://doi.org/10.1016/j.celrep.2020.02.091.

[31] K. Luszczynski, et al., Markers of dermal fibroblast subpopulations for viable cell isolation via cell sorting: a comprehensive review, Cells 13 (2024), https://doi.org/10.3390/cells13141206.
[32] B.D. Manning, L.C. Cantley, AKT/PKB signaling: navigating downstream, Cell 129 (2007) 1261–1274, https://doi.org/10.1016/j.cell.2007.06.009.
[33] Q. Yao, et al., Neurotrophin 3 upregulates proliferation and collagen production in human aortic valve interstitial cells: a potential role in aortic valve sclerosis, Am. J. Physiol. Cell Physiol. 312 (2017) C697–C706, https://doi.org/10.1152/ajpcell.00292.2016.
[34] C.H. Jeong, et al., Phosphorylation of Sox2 cooperates in reprogramming to pluripotent stem cells, Stem Cell. 28 (2010) 2141–2150, https://doi.org/10.1002/stem.540.
[35] D. Chouhan, B.B. Mandal, Silk biomaterials in wound healing and skin regeneration therapeutics: from bench to bedside, Acta Biomater. 103 (2020) 24–51, https://doi.org/10.1016/j.actbio.2019.11.050.
[36] R. Ziadlou, et al., Optimization of hyaluronic acid-tyramine/silk-fibroin composite hydrogels for cartilage tissue engineering and delivery of anti-inflammatory and anabolic drugs, Mater Sci Eng C Mater Biol Appl 120 (2021) 111701, https://doi.org/10.1016/j.msec.2020.111701.
[37] Y. Jing, et al., Regenerated silk fibroin and alginate composite hydrogel dressings loaded with curcumin nanoparticles for bacterial-infected wound closure, Biomater. Adv. 149 (2023) 213405, https://doi.org/10.1016/j.bioadv.2023.213405.
[38] C. Liang, et al., Synthesis and characterization of silk fibroin-MXene composite electrospun fibers for biomedical applications, Front. Chem. 12 (2024) 1471148, https://doi.org/10.3389/fchem.2024.1471148.
[39] O. Chaudhuri, et al., Hydrogels with tunable stress relaxation regulate stem cell fate and activity, Nat. Mater. 15 (2016) 326–334, https://doi.org/10.1038/nmat4489.
[40] X. Kong, et al., Biomimetic hydrogel for rapid and scar-free healing of skin wounds inspired by the healing process of oral mucosa, Acta Biomater. 100 (2019) 255–269, https://doi.org/10.1016/j.actbio.2019.10.011.
[41] J.D. Parkin, et al., The collalphagen III fibril has a "flexi-rod" structure of flexible sequences interspersed with rigid bioactive domains including two with hemostatic roles, PLoS One 12 (2017) e0175582, https://doi.org/10.1371/journal.pone.0175582.
[42] M. Xue, C.J. Jackson, Extracellular matrix reorganization during wound healing and its impact on abnormal scarring, Adv. Wound Care 4 (2015) 119–136, https://doi.org/10.1089/wound.2013.0485.
[43] X. Liu, H. Wu, M. Byrne, S. Krane, R. Jaenisch, Type III collagen is crucial for collagen I fibrillogenesis and for normal cardiovascular development, Proc. Natl. Acad. Sci. USA 94 (1997) 1852–1856, https://doi.org/10.1073/pnas.94.5.1852.
[44] S.W. Volk, Y. Wang, E.A. Mauldin, K.W. Liechty, S.L. Adams, Diminished type III collagen promotes myofibroblast differentiation and increases scar deposition in cutaneous wound healing, Cells Tissues Organs 194 (2011) 25–37, https://doi.org/10.1159/000322399.
[45] J. Simkin, et al., Epidermal closure regulates histolysis during mammalian (Mus) digit regeneration, Regeneration (Oxf) 2 (2015) 106–119, https://doi.org/10.1002/reg2.34.
[46] N.H. Gopee, et al., A prenatal skin atlas reveals immune regulation of human skin morphogenesis, Nature 635 (2024) 679–689, https://doi.org/10.1038/s41586-024-08002-x.
[47] D.C. Stewart, et al., Type III collagen regulates matrix architecture and mechanosensing during wound healing, J. Invest. Dermatol. 145 (2025) 919–938 e914, https://doi.org/10.1016/j.jid.2024.08.013.
[48] C. Kiratipaiboon, et al., SOX2Mediates carbon nanotube-induced fibrogenesis and fibroblast stem cell acquisition, ACS Biomater. Sci. Eng. 6 (2020) 5290–5304, https://doi.org/10.1021/acsbiomaterials.0c00887.
[49] S.H. Sun, H.H. Fan, X.W. Wang, B.D. Bing, Y.J. Hu, Platelet-rich fibrin attenuates inflammation and fibrosis in vulvar lichen sclerosus via the TGF-beta/SMAD3 pathway, Arch. Dermatol. Res. 317 (2025) 360, https://doi.org/10.1007/s00403-025-03811-0.
[50] Y. Li, et al., Macrophage-myofibroblast transition contributes to the macrophage elimination and functional regeneration in the late stage of nerve injury, Exp. Neurol. 387 (2025) 115194, https://doi.org/10.1016/j.expneurol.2025.115194.
[51] J. Lu, Z. Wang, L. Zhang, Single-cell transcriptome analysis revealing mechanotransduction via the Hippo/YAP pathway in promoting fibroblast-to-myofibroblast transition and idiopathic pulmonary fibrosis development, Gene 943 (2025) 149271, https://doi.org/10.1016/j.gene.2025.149271.